Summary from the 1st AIAA Ice Prediction Workshop

Eric Laurendeau, Simon Bourgault-Cote, Isik Ozcer, Richard Hann,
Emmanuel Radenac, Alberto Pueyo

Summary from the 1st AIAA Ice Prediction Workshop

É. Laurendeau* and S. Bourgault-Côté.†
Polytechnique Montréal, Montréal, Québec, H3T 1J4, Canada

I. Ozcer‡
ANSYS Canada, Montréal, Québec, H3A 3G4, Canada

R. Hann§
Norwegian University of Science and Technology, Trondheim, 7491, Norway

E. Radenac¶
ONERA / DMPE, Université de Toulouse, F-31055 Toulouse, France

A. Pueyo‖
Bombardier, Dorval, Québec, H4S 1Y9, Canada

The AIAA 1st ice prediction workshop focused on establishing current 2D and 3D simulation capabilities towards ice accretion on aircraft by bringing together scientists from diverse backgrounds such as code developers, experimentalists and users. To that end, experimentally and publicly available rime and glaze ice accretion data were provided for a wide range of applications. The geometries include single and multi-element airfoils, wings, engine inlet and horizontal tail configurations in flow with different droplet size distributions including Supercooled Large Droplets. In addition to ice accretion, data such as pressure distribution, ice mass and collection efficiency were provided, when available. Results from various Computational Fluid Dynamics workflows were provided by academia, research/federal centers and industries. The submitted data is analyzed via code-to-code and code-to-experiment comparison plots. While the many comparisons are now publicly available, the paper presents the detailed analysis on some selected baseline and optional cases. A methodology and technology gap assessment concludes on the current state-of-the-art and presents possible future workshops directions to improve our understanding and modeling of the various phenomena at play.

I. Nomenclature

β	=	Collection efficiency
LWC	=	Liquid water content
MAC	=	Mean aerodynamic chord
MVD	=	Median volume diameter

II. Introduction

The idea of an ice prediction workshop stems from the SAE AC-9C meeting in Reno, Nevada, on October 16, 2018. Then, several persons reckoned that the community would benefit from an additional benchmarking activity to the seminal NATO RTO Technical Report entitled 'Ice Accretion Simulation Evaluation test' produced by the Applied Vehicle Technology panel Task Group AVT-006 in 2001 [1]. Indeed, the two decades following this workshop saw

*Professor, Mechanical Engineering Department, eric.laurendeau@polymtl.ca, AIAA Senior Member.
†Research Professional, Mechanical Engineering Department, AIAA Member.
‡Lead R&D engineer.
§Researcher, Engineering Cybernetics.
¶Research Engineer, Multi-physics department for energy.
‖Senior Engineering Specialist, Advanced Aerodynamics.

tremendous developments in CFD within all aspects of the numerical workflow as well as experimental data acquisition techniques. Hence, a new assessment of the state-of-the-art towards ice accretion on aircraft was confirmed during the SAE AC-9C meeting held in Minneapolis, Minnesota, on June 17, 2019 in conjunction with the SAE International Conference on Icing of Aircraft, Engines, and Structures. There, an assembled committee of volunteers committed to enact such event and held a kick-off meeting on November 20, 2019 with the goal of holding the first of many future workshops in conjunction with the summer AIAA 2021 Aviation Forum.

Table 1 AIAA 1^{st} ice prediction workshop committee (alphabetical)

Name (alphabetical)	Institution or company
Phil Alldridge	Phil Alldridge Sikorsky, Lockheed
Roger Aubert	Bell Flight
Galdemir Botura	Collins Aerosapce
Simon Bourgault-Côté	Polytechnique Montréal
Andy Broeren	NASA
Julien Cliquet	Airbus
Don Cook	Boeing
Guy Fortin	Bombardier
Richard Hann	Norwegian University of Science and Technology
Bryan Hinson	Textron Aviation
Eric Laurendeau	Polytechnique Montréal
Adam Malone	Boeing
Richard Moser	Aerotex
Karthik Narayanasamy	Honeywell
Isik Ozcer	Ansys
Ezgi Oztekin	FAA
Chris Nelson	Siemens
Mark Potapczuk	NASA
Alberto Pueyo	Bombardier
Emmanuel Radenac	ONERA
Durrell Rittenberg	Siemens
Krysztof Szilder	National Research Council
William Wright	HX5, LLC
Kevin Yugulis	Battelle

The committee, under the leadership of Dr. Broeren of NASA, operated in transparency with membership growing to 24 members from diverse affiliations (e.g., academia, research/federal centers, industries) as listed in Table 1. The members geographical footprint includes the Americas and Europe. In addition to this, 13 more people were on the committee mailing list and occasionally participated in the bi-weekly meetings. Understanding the complexity of the multiphysics problems and inspired by the series of highly successful AIAA workshops (drag, high-lift, aeroelastic, etc.), the committee privileged a long-term approach targeting several successive icing workshops. Hence, for the inaugural AIAA event, it was decided to restrict the exploration space to produce a state-of-the art benchmarking activity that would serve as a stepping-stone to future workshops. First, cases similar to the ones of the NATO 2001 report would allow measuring the progress made in two decades. Then, multi-element cases would examine the performance on complex geometry and additional flow physics such as airfoil wakes and shadow zones. Finally, 3D shapes such as wings, horizontal tails and engine inlets would assess the performance of 3D frameworks, let alone if the development of rigorous 3D quantitative metrics can be established. Analysis of participants results would serve to establish the diversity of the methods and their accuracy as well as to identify technology gaps. These would help plan future efforts whether these would be experimental, modeling, or numerical in nature. Therefore, the 1st ice prediction workshop

objectives can be summarized as:

- Focus on assessment of current icing simulation capabilities for ice shapes on both 2D and 3D geometries based on publicly available experimental data for rime/glaze conditions, including Supercooled Large Droplets (SLD) cases.
- Assess numerical workflows through (i) baseline cases, for airfoil and wing configurations with Appendix C conditions and (ii) optional cases with Appendix O conditions and other geometries. Compare results on several key metrics, such as airflow, collection efficiency, freezing fraction, ice mass, ice thickness, etc. Some meshes were provided by the committee to the participants and no particular effort was spent on analyzing the effects of different meshes.
- Develop methods to perform quantitative comparisons, especially for 3D results. Encourage discussions about the definition of metrics applicable to 3D ice accretion analysis.
- Analyze the results of the first workshop to identify cases for future workshops including how to gather experimental data from different facilities, possibilities for 'blind' comparisons and expansion into other problems such as engine icing, rotorcraft, ice protection systems, probes, etc.

The paper presents the test cases and shows a large overview of the results discussed during the workshop. Indeed, it would have been impossible to show and analyze all the results, available on the workshop website. It analyzes the results obtained by the participants in view of the workshop objectives.

III. Test Cases and Experimental Data

The committee provided 8 baseline and 8 optional cases, from 2D single- and multi-element airfoils to 3D wings and engine inlet with corresponding experimental data. A top-level summary of the cases is presented in Table 2, with 3 categories encompassing 7 geometries. For each category (1 to 3), several test cases were identified and tagged with two additional digits. Together, they form 3-digit test case identifiers named 'case-xyz', with 'x' being the category, 'y' the configuration and 'z' the counter for the Baseline and/or Optional case ranging between 1 and 4.

Table 2 Baseline and optional cases

Category	Configuration	Baseline	Optional
1. Droplet Impingement	1. NACA 64A008 finite swept tail	1	1
	2. Multi-element airfoil	1	1
	3. Axisymmetric inlet	0	2
2. Ice accretion 2D	4. 18-inch chord NACA23012	2	0
	5. 72-inch chord NACA23012	0	2
3. Ice accretion 3D	6. NACA 0012, 30 degrees sweep	2	2
	7. NACA 0012, 45 degrees sweep	2	0

A. Category 1: Droplet impingement

1. Case 111 and 112

The baseline and optional cases, taken from reference 2, concern the NACA 64A008 swept tail at 6-degree angle-of-attack with droplets of median volume diameters (MVD) equal to 21 and 92 microns, respectively. The flow conditions are as follows:

- Speed: 78.68 m/s
- Mach: 0.23
- Mean Aerodynamic Chord (MAC): 0.9563 m or 36 inches
- Reynolds number based on MAC: 5 million
- Static temperature: 280 K
- Static pressure: 95147 Pa
- 27-bin droplet distribution

The sectional data taken from strip-A located 36 inches from the tunnel floor is used for the comparisons. The

experimental geometry and surface pressure distribution are shown in Fig. 1, while the experimental β-distributions (with one numerical prediction) are shown in Fig. 2 below.

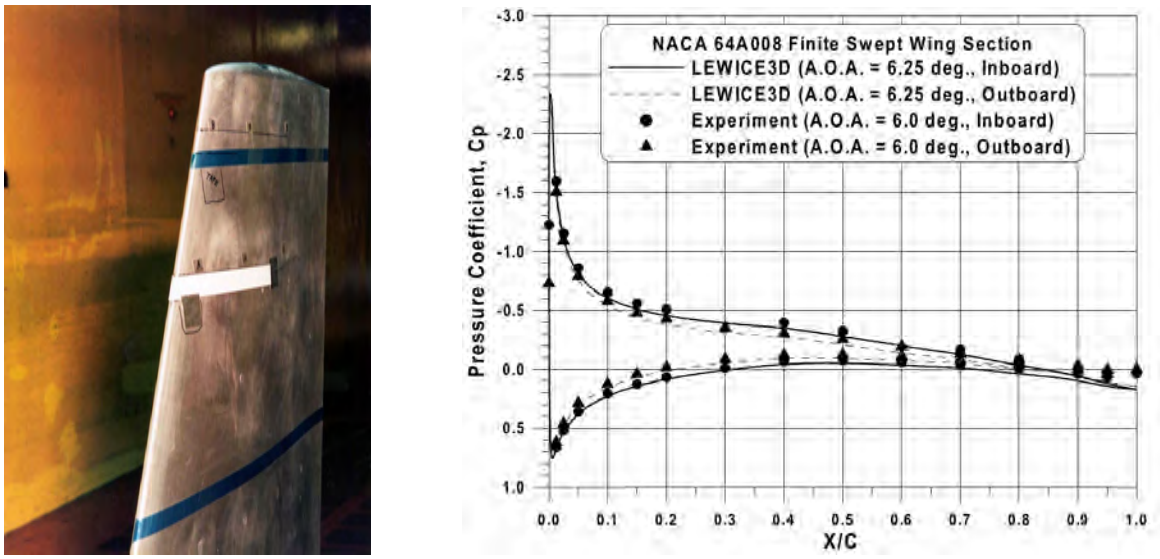

(a) Tail experimental model. **(b) Pressure distribution.**

Fig. 1 Case 111/112 geometry (left) and clean wing surface pressure distribution (right) [2].

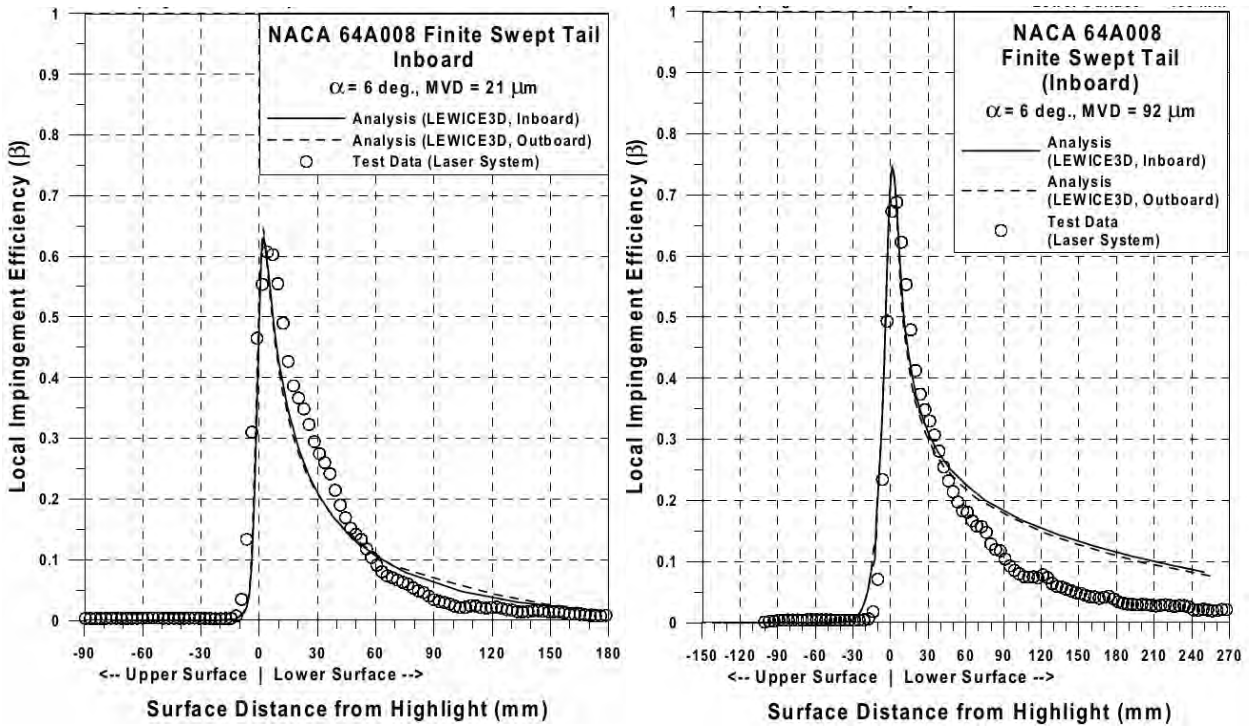

Fig. 2 Cases 111 (left) and 112 (right) surface β–distributions [2].

2. Case 121/122

The baseline and optional cases, taken from reference 2, concern a three–element airfoil at 4-degree angle–of–attack with median droplet diameters of 21 and 92 microns, respectively. The flow conditions are as follows:

- Speed: 78.2 m/s
- Mach: 0.23
- Mean Aerodynamic Chord (mac): 0.9563 m or 36 inches
- Reynolds number based on mac: 4.9 million
- Static temperature: 278 K
- Static pressure: 95630 Pa
- 27-bin droplet distribution

The geometry and the β-distributions for the 21- and 92-micron cases are respectively shown in Fig. 3 to 5.

Fig. 3 Case 121/122 three–element airfoil in icing tunnel (rotated, downstream) [2].

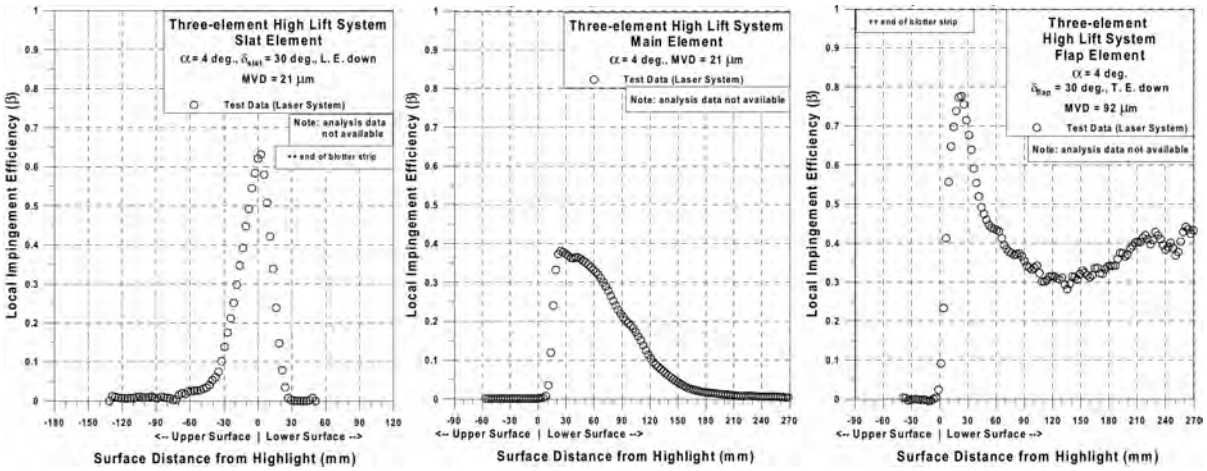

(a) Slat element. **(b) Main element.** **(c) Flap element.**

Fig. 4 Case 121, β–distribution over three–element airfoil, MVD 21 microns [2].

3. Case 131/132

The two optional cases, taken from [3], concern an axisymmetric nacelle at 15-degree angle-of-attack with droplets of median volume diameter (MVD) of 20.36 microns, at a mass flow of 7.8 kg/s and 10.41 kg/s, respectively. The case conditions are as follows:

- Mach: 0.2328

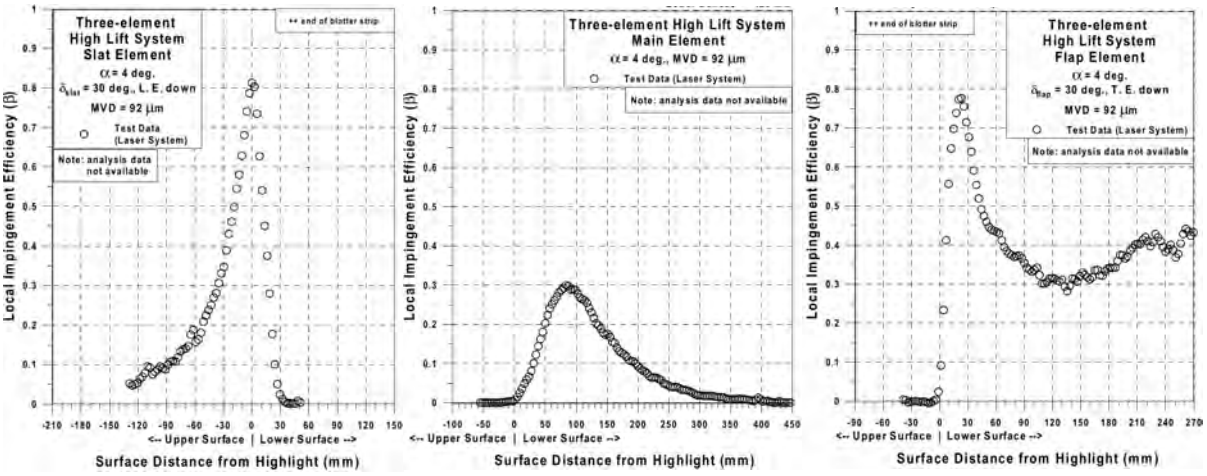

(a) Slat element. **(b) Main element.** **(c) Flap element.**

Fig. 5 Case 122, β–distribution over three–element airfoil, MVD 92 microns [2].

- Static temperature: 283.15 K
- Static pressure: 95492 Pa
- Single droplet size

The geometry on which the azimuthal angles are defined is shown in Fig. 6. The surface pressure measurements at 180, 90 and 0 degrees are shown in Fig. 7 for the 7.8 and 10.4 kg/s mass rates, respectively on top and bottom. Finally, the β–distributions at several locations around the nacelle for the 7.8 and 10.41 kg/s cases are shown in Fig. 8 and 9 respectively. Note that the calculated data provided from the NASA report is the result of an aerodynamic panel code providing the inviscid flow field as an input to a Lagrangian droplet method.

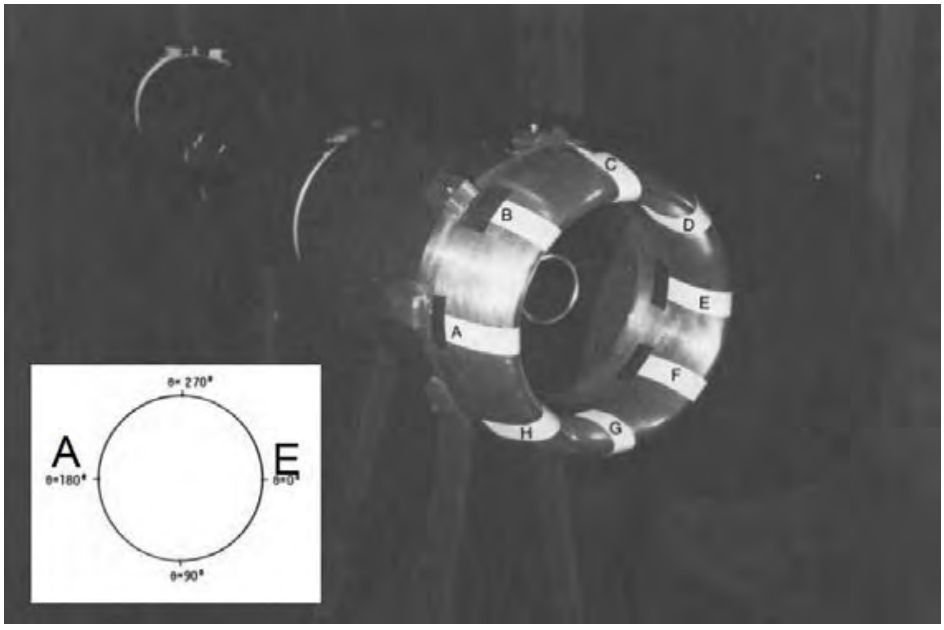

Fig. 6 Experimental blowdown nacelle geometry [3].

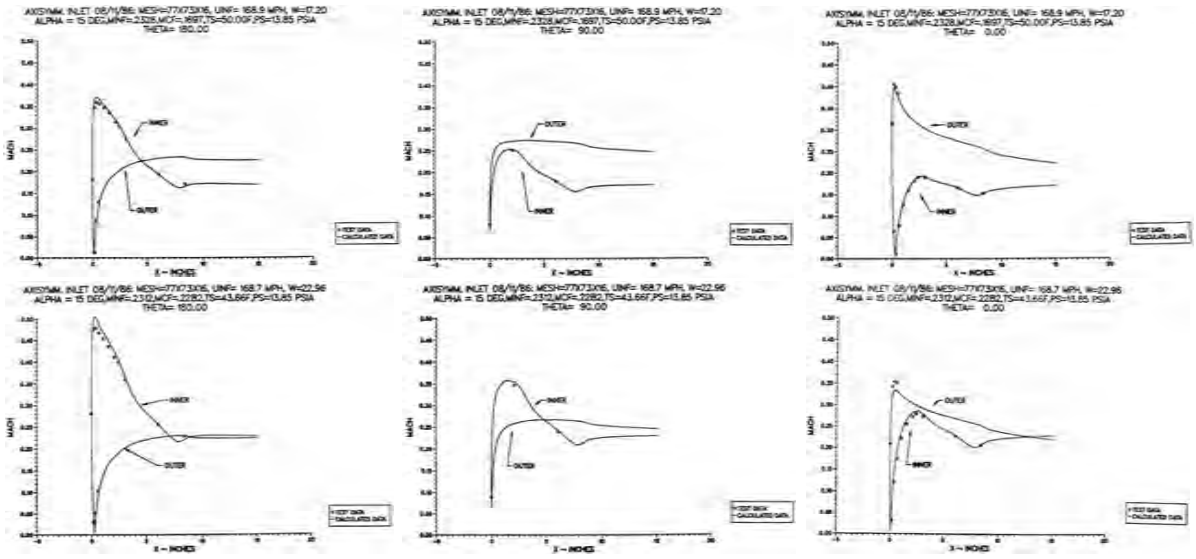

Fig. 7 Experimental and numerical (Panel method) surface isentropic Mach numbers (top 7.8 kg/s, bottom 10.41 kg/s) [3].

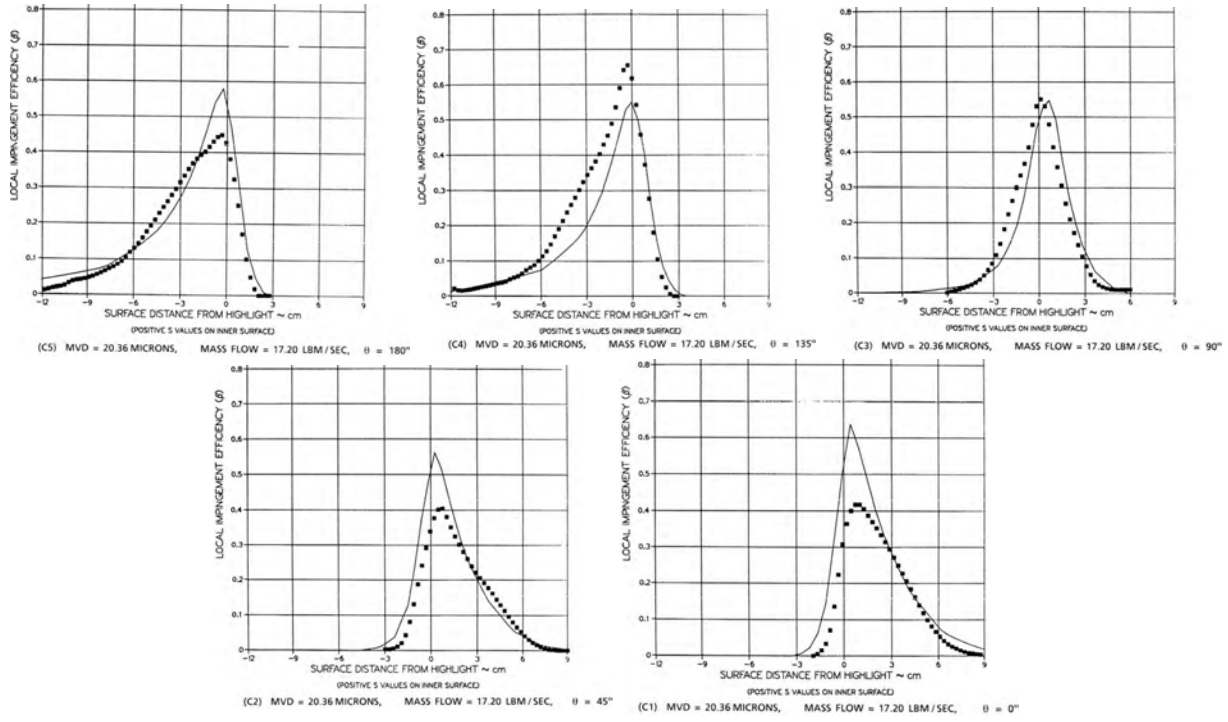

Fig. 8 Experimental and numerical (Lagrangian) surface β–distribution for case 131 (7.8 kg/s) [3].

B. Category 2: Ice accretion 2D

1. Cases 241/242

The two baseline cases, one in rime and one in glaze conditions are taken from [4]. They concern an 18-inch NACA23012 airfoil at 2-degree angle-of-attack. The flow conditions are as follows:

- Case 241, rime ice
  - Tunnel run ED1977

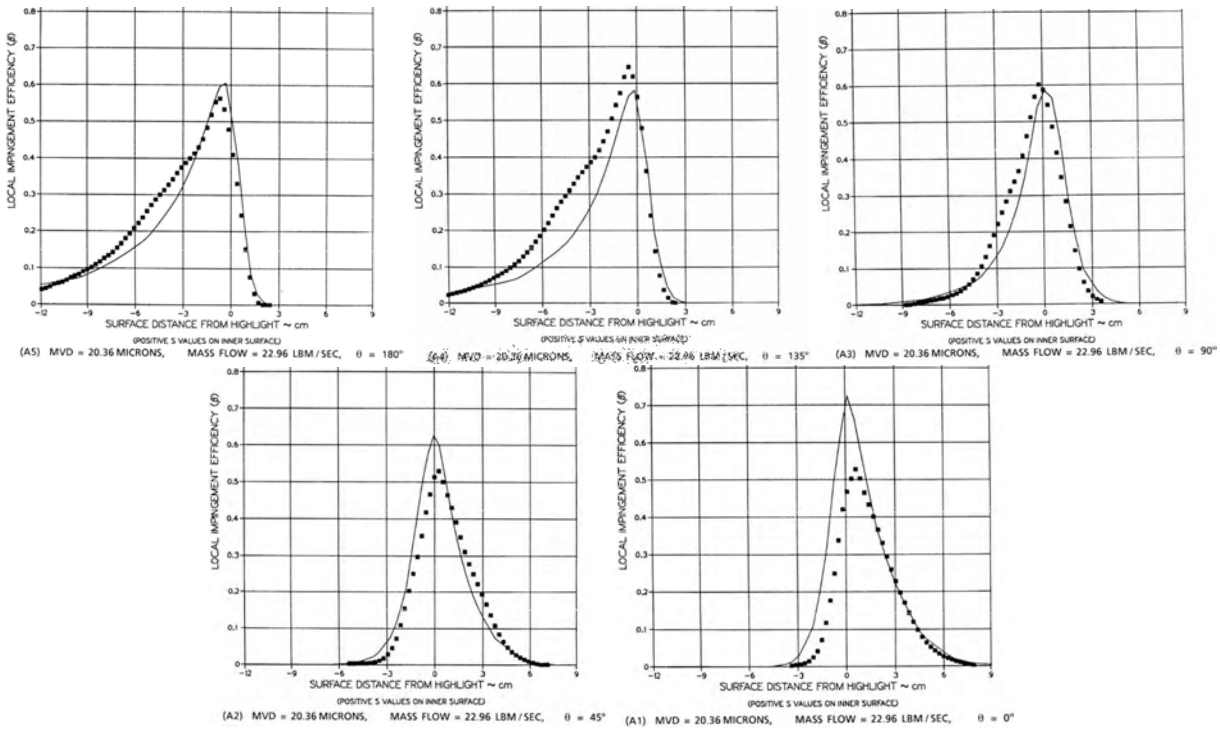

Fig. 9 Experimental and numerical (Lagrangian) surface β–distribution for case 132 (10.41 kg/s) [3].

  - MVD: 30 microns
  - LWC: 0.42 g/m3
  - Speed: 103 m/s
  - Mach: 0.325
  - Total temperature: -17.8 C
  - Static temperature: -23 C
  - Static pressure: 92528 Pa
  - Mean Aerodynamic Chord (MAC): 0.4572 m or 18 inches
  - Reynolds number based on MAC: 4.9 million
  - A 7-bin distribution representative of the droplet-size distribution in the IRT wind tunnel was provided
  - Spray time: 5 minutes
- Case 242, glaze ice
  - Tunnel run ED1978
  - MVD: 15 microns
  - LWC: 0.81 g/m3
  - Speed: 103 m/s
  - Mach: 0.31
  - Total temperature: -1.9 C
  - Static temperature: -7.1 C
  - Static pressure: 92941 Pa
  - Mean Aerodynamic Chord (MAC): 0.4572 m or 18 inches
  - Reynolds number based on MAC: 3.4 million
  - A 7-bin distribution representative of the droplet-size distribution in the IRT wind tunnel was provided
  - Spray time: 5 minutes

The geometry in the tunnel section is shown in Fig. 10 and scan slices at the end of the 5-minutes period of the geometry are shown in Fig. 11 for both cases (scans or tracings). Since the ice accretion varies with the span, different experimental data extraction techniques produce different ice shapes. Differences for rime ice are small, as expected, whereas for glaze ice they can be significant as shown by Fig. 12. To better understand the discrepancies, NASA results

on various repeats confirmed the presence of the two horns, with an invariant stagnation region ice thickness [4]. The horns' thicknesses, however, vary in size but have similar position in the convex stagnation region, as shown in Fig. 13. In-tunnel photographs of run ED1978 are shown in Fig. 14.

Fig. 10 36-inch NACA23012 Airfoil in icing tunnel (rotated) [4].

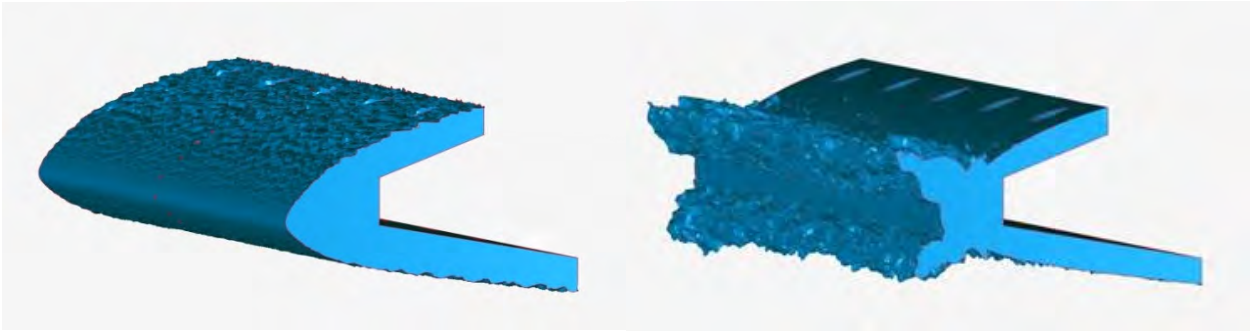

Fig. 11 Experimental 3D ice accretion scans for case 241 (left) and 242 (right) [4].

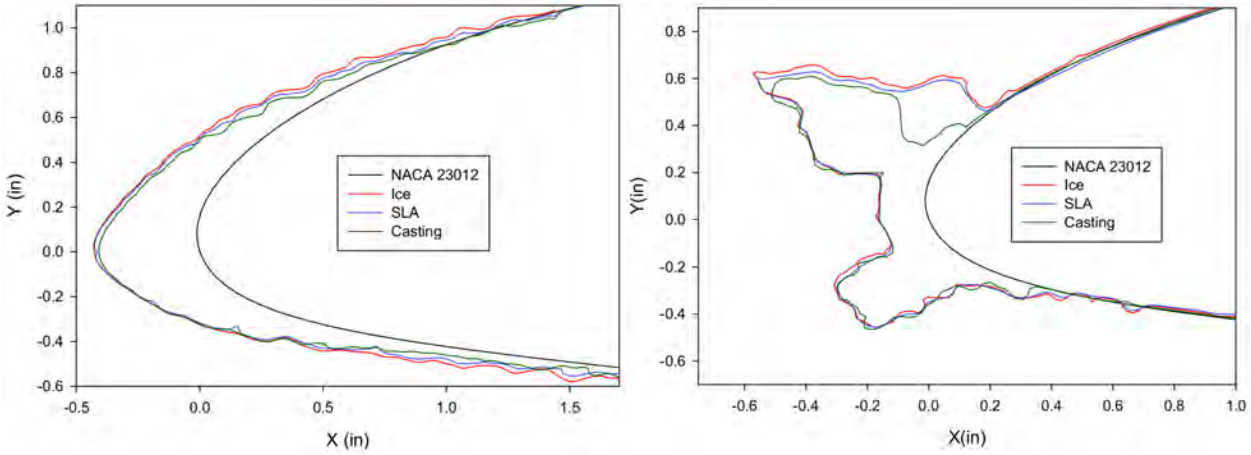

Fig. 12 Experimental ice accretion post-processed sections for case 241 (left) and 242 (right) using various extraction techniques [4].

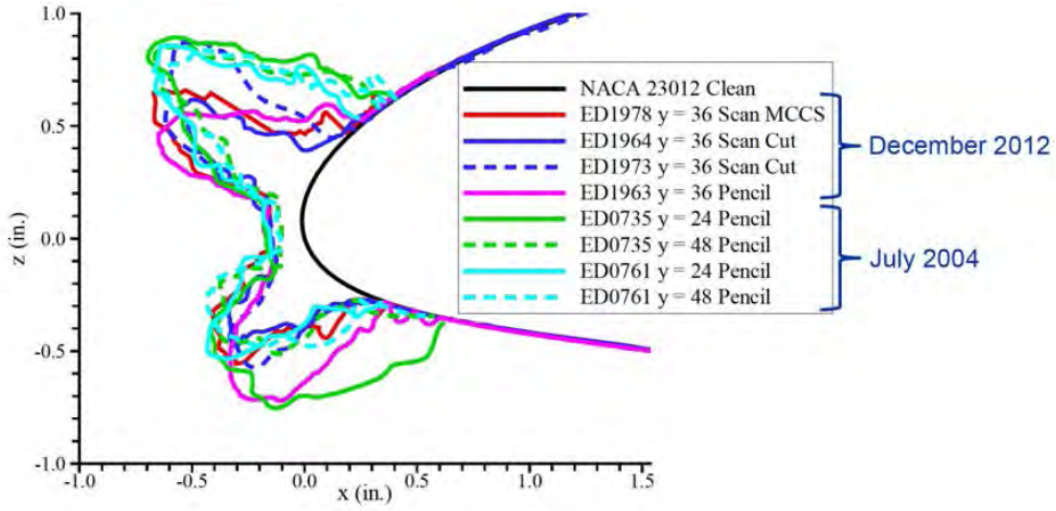

Fig. 13 Experimental ice thickness for repeated runs of Case 242*.

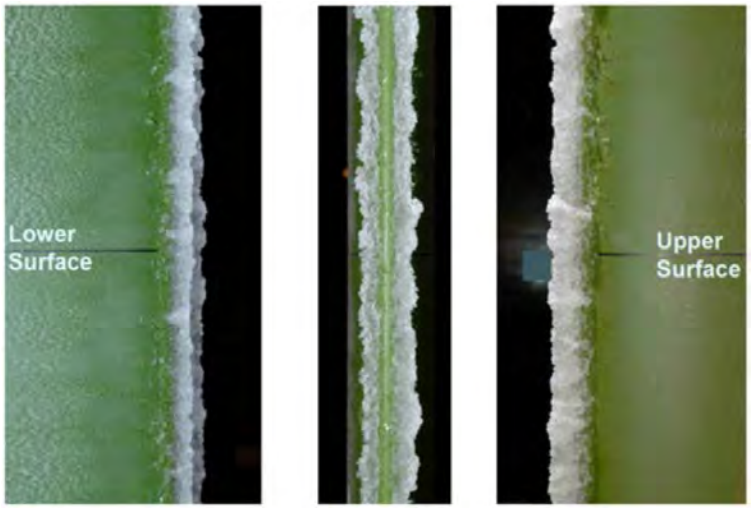

Fig. 14 Experimental ice accretion photographs for case 242, run ED1978*.

2. Case 251/252

The two optional cases, taken from [5], differ in that they use a monomodal and bimodal droplet distribution, respectively. Both concern a 72-inch NACA23012 airfoil at a 2-degree angle-of-attack. The case conditions are as follows:

- Tunnel runs ED2819 and ED2820, respectively for case 251 (monomodal distribution) and 252 (bimodal distribution)
- MVD: 21.5 microns
- LWC: 1.64 g/m3
- Speed: 103 m/s
- Total temperature: -7.3 C
- Static temperature: -12.6 C
- Static pressure: 91700 Pa
- Mean Aerodynamic Chord (MAC): 1.829 m or 72 inches

*Private communication, Andy Broeren, used with permission, 27 July 2021.

• Spray time: 6.63 minutes

The geometry in the tunnel is shown in Fig. 15, while the extracted ice accretion shapes for both cases are shown in Fig. 16. Additional experimental data provides variations of ice mass, ice volume and ice density with their corresponding percentage differences as shown in Table 3.

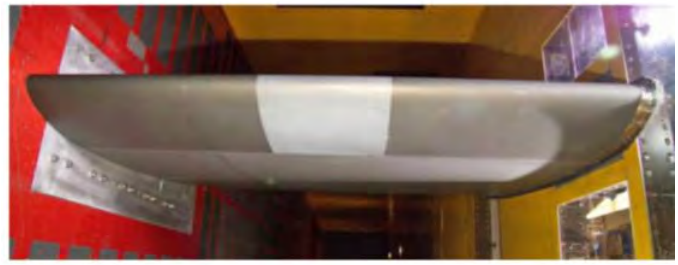

Fig. 15 72-inch NACA23012 Airfoil in icing tunnel (rotated) [5].

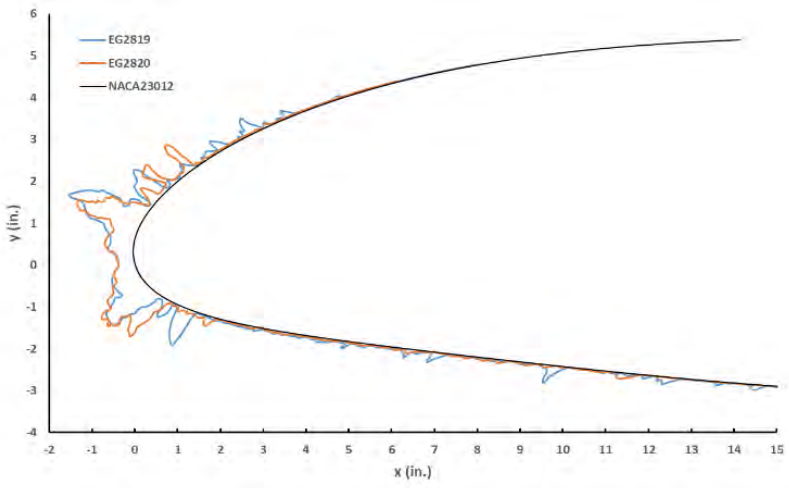

Fig. 16 Experimental ice accretion post-processed sections mid-span for case 251 and 252 [5].

Table 3 Additional Experimental data characterizing the ice accretion [5].

Case	Mass bimodal (g)	Mass monomodal (g)	ΔM (g)	ΔM (%)	Volume bimodal (in^3)	Volume monomodal (in^3)	ΔVolume (in^3)	ΔVolume (%)	Eff. density bimodal (g/cm^3)	Eff. density monomodal (g/cm^3)	ΔEffective density (%)
251/252	667.0	549.6	117.4	21.4	52.47	43.07	9.40	21.8	0.776	0.779	-0.4

C. Category 3: Ice accretion 3D

1. Cases 361 / 362 / 363 / 364

These cases all refer to the NACA0012 30-degree swept wing, taken from [6]. The first two cases are baseline ones, while the last two are optional. Cases 361 and 362 only differ by the static temperature settings which correspond to rime and glaze ice conditions respectively, as follows:

- Tunnel runs AF2146 (case 361), AF2145 (case 362), AF2881 (case 363) and AF2892 (case 364)
- MVD: 34.7 microns (cases 361, 362), 20.5 microns (cases 363, 364)
- LWC: 0.50 g/m^3
- Speed: 103 m/s (cases 361, 362), 115.24 m/s (case 363), 114.21 m/s (case 364)
- Static temperature: 257K (case 361), 266K (case 362), 263.2K (case 363), 259.8 K (case 364)
- Static pressure: 92321 Pa (cases 361, 362), 90321 Pa (case 363), 89632 Pa (case 364)
- A 7-bin distribution representative of the droplet-size distribution in the IRT wind tunnel was provided
- Spray time: 20 minutes (cases 361, 362), 17.7 minutes (cases 363, 364)

The half-model geometry in the tunnel is shown in Fig. 17. Spanwise and frontal views of the rime and glaze ice shapes are shown in Fig. 18 and 19, respectively.

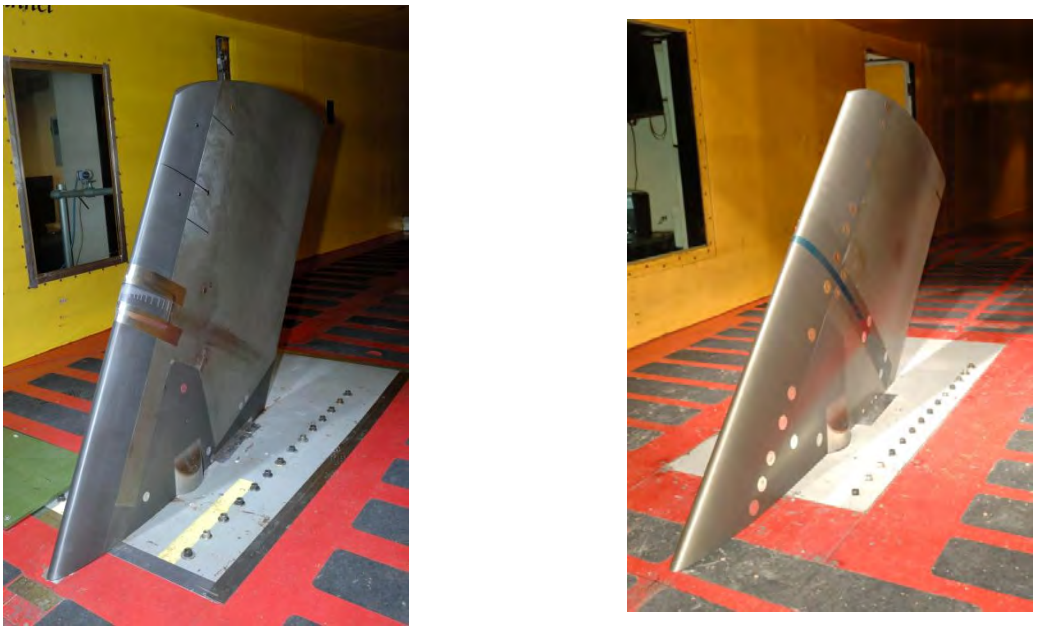

Fig. 17 30– (left) and 45–degree (right) swept NACA0012 wing in icing tunnel [6].

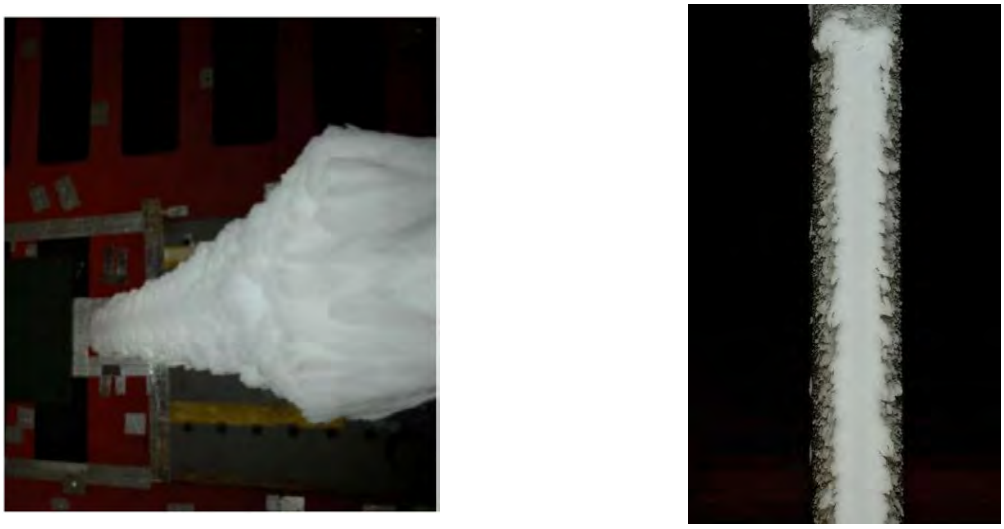

Fig. 18 Spanwise and frontal views of experimental ice accretion, case 361 (rime) [6].

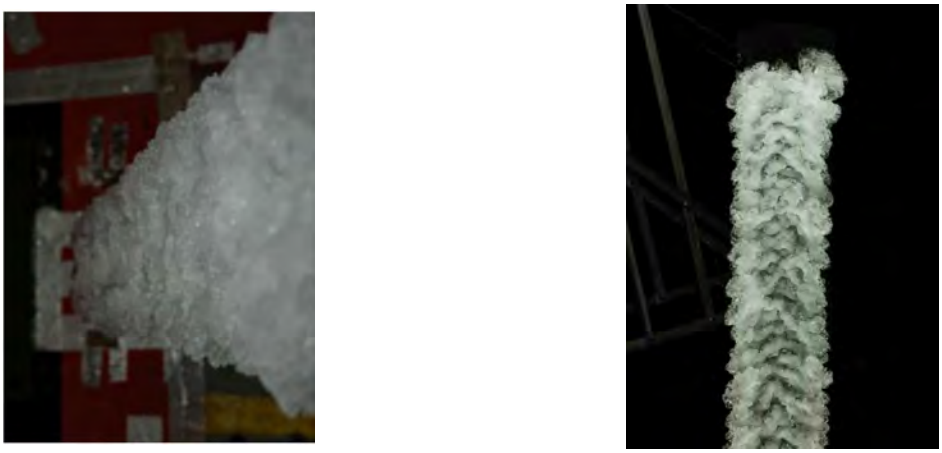

Fig. 19 Spanwise and frontal views of experimental ice accretion, case 362 (glaze) [6].

2. Cases 371/372

The two baseline cases, taken from [7], target flows over highly swept wings that see ice accretion with 'lobster tail' topologies. The first case corresponds to rime ice whereas the second one is in glaze ice conditions. They differ in their static temperature, which are respectively 257K and 266K. Both concern a 45-degree swept wing with NACA0012 airfoil sections that is mounted as a half-span model at 0-degrees angle-of-attack. The flow conditions are as follows:

- Tunnel run AF1799 and AF1795, respectively for case 371 and 722
- MVD: 32 microns
- LWC: 0.50 g/m^3
- Speed: 103 m/s
- Static pressure: 94463 Pa
- Spray time: 20 minutes

The geometry in the tunnel is shown in Fig. 17. Spanwise and frontal views of the rime and glaze ice shapes are shown in Fig. 20 and 21 respectively, with the glaze ice 'lobster tail' or 'scallops' showing clearly for both icing conditions.

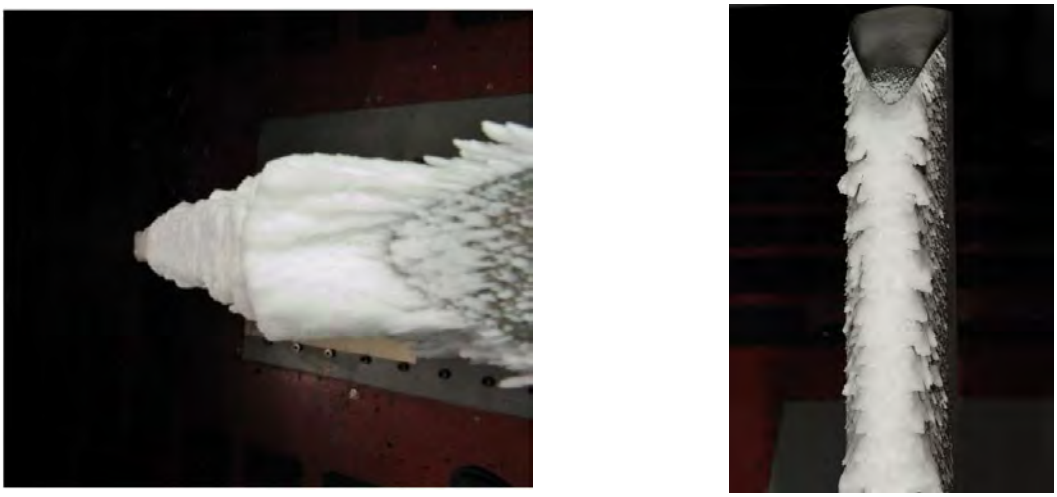

Fig. 20 Spanwise and frontal views of experimental ice accretion, case 371 (rime) [7].

Fig. 21 Spanwise and frontal views of experimental ice accretion, case 372 (glaze) [7].

IV. Post-Processing Maximum Combined Cross-Section (MCCS)

When comparing numerical and experimental ice shapes, several kinds of analyses can be made. For several 2D cases, basic tracings can be provided and compared to the ice shapes produced by the codes. Molding or scanning techniques can also be used for such comparisons. When analyzing 3D data, the observed spanwise variations bring an additional challenge when extracting experimental data. As more CFD workflows tackle 3D ice accretion, whether via deterministic or non-deterministic (i.e., morphogenetic [8] or stochastic [9]) models, the same must be done when extracting numerical data. Although the whole experimental geometry can be superimposed on the numerical geometry after triangularization, simplified representations of the ice shape are searched. The work of Broeren et al. [10] introduced the documentation technique for performing MCCS extraction from experimental data. The process is illustrated in Fig. 22, taken from [10]. In essence, a given spanwise section is scanned and sectional ice shapes extracted at discrete position within the interval. The MCCS corresponds to the outermost region of the combined individual sections.

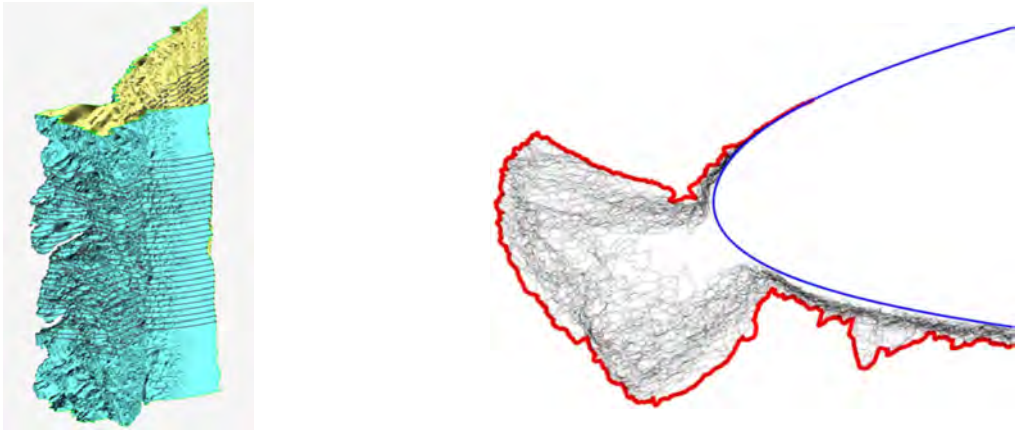

Fig. 22 Maximum Combined Cross Section (MCSS) process for scanned ice shapes [10].

A similar process was devised for extraction of CFD results by Dr. Ozcer, from ANSYS, for constant chord swept wings, which corresponds to the swept wings test cases of the workshop. First, a solid body rotation is performed normal to the wing plane to arrive at a zero-swept wing in the transformed space. Then, the same process as in [10] discussed above is performed. The process involves additional steps as shown in Fig. 23. For the extracted discrete span range, one creates a uniform scalar of value 1 in the volume surrounding the ice. Then, interpolation to the selected

slice is performed to get 0 or 1 values identifying the ice boundary for that section. Then, a simple summation of the scalar is made and rescaled by the number of slices to again fall for a range of 0 (inside) to 1 (outside). This process resembles the approach of Pena et al. [11] using the signed level set function, but in the discrete space rather than the continuous one. Note that the extracted data can be reordered as an ordered data set, so that visualization packages can plot a continuous MCCS line in addition to discrete points.

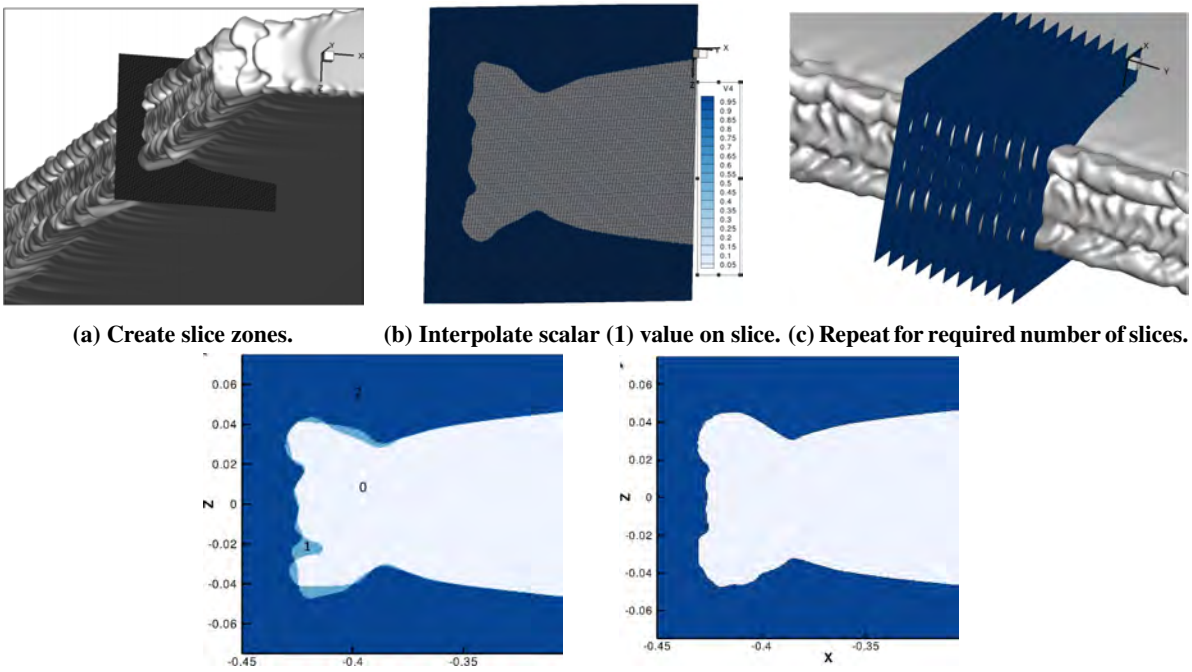

(a) Create slice zones. **(b) Interpolate scalar (1) value on slice.** **(c) Repeat for required number of slices.**

(d) Sum the values from all slices. **(e) Rescale by number of slices to recover MCCS.**

Fig. 23 Maximum Combined Cross Section (MCSS) process proposed for CFD ice shapes.

V. Overview of Submitted Data and Methods Used

The workshop saw 21 teams submitting data to Polytechnique Montreal, who acted as the repository of all results to enable comparisons. A workshop data flow process was defined, under the leadership of Dr. Bourgault-Côté of Polytechnique Montréal, through several iterative rounds with the workshop committee. The work necessitated the creation of a dedicated 'Data Analysis Workforce' and a custom postprocessing automated Python script to provide the final comparisons.

Many participants used several workflows depending on the test case. For instance, legacy 2D workflows, such as potential flow solvers with/without boundary-layer coupling, are still used. Some groups showed novel algorithms, such as the immersed boundary method or very recent RANS solvers in addition to their baseline workflows. Some presentations did not explicitly list their entire workflows. Quantitative workflow metrics are extracted to provide a mapping of the methods used, so that we can statute on the state-of-the-art. The committee purposely did not enforce any standards for the presentations, except for the data comparisons, so that one can extract what is considered 'standards' and what is still 'non-standard' processes by inspecting common threads in all presentations. Note that because some groups used many workflows and some do not list their entire process, the sum of the metrics can exceed or be smaller than the 21 data entries.

Of the 21 presentations, which each contained several baseline and/or optional test cases with different versions of their specific workflows, all but one used RANS for their aerodynamic flow solution. This is a remarkable change from the 2001 NATO/RTO workshop. Five groups complemented these results with potential methods in 2D. Also 5 groups used 2D results on potential flow or RANS solutions adjusted with infinite swept wing corrections for 3D cases. When using RANS, all reported the turbulence model used except two groups. Only one group reported a RANS

model with wall-functions. The models were either SA (Spalart and Allmaras [12]) or k-w-SST (Menter [13] or some variations thereof) and several used variants with wall roughness to increase the heat transfer over the iced surface. Five groups included the effect of laminar-turbulent transition, either via boundary-layer code (e.g. [14]) or correlation-based transitional RANS models (eg. [15]).

Table 4 Participant information sumary.

ID	Participant	Code	ID	Participant	Code
01.1	Boeing	LEWICE	10.4	AIT	CFX/ICEAC2D
01.2	Boeing	LEWICE3D	10.5	AIT	Fluent/FENSAP-ICE
03.1	NASA	GlennICE	10.6	AIT	Fluent/FENSAP-ICE
03.2	NASA	LEWICE	10.7	AIT	Fluent/FENSAP-ICE
03.3	NASA	LEWICE	11.1	NTNU	FENSAP-ICE
04.1	ONERA	IGLOO3D	11.2	NTNU	FENSAP-ICE
04.2	ONERA	IGLOO2D	12.1	NRC	Cobalt
05.1	GeorgiaTech	ANSYS Fluent/GTDROP-Uns/GT-ICE	13.1	Ansys-Bombardier	FENSAP-ICE
06.1	PolitechnicoDiMilano	SU2/PoliDrop/PoliMIce	13.2	Ansys-Bombardier	FENSAP-ICE
07.1	Textron	USM3D/LEWICE/LEWICE3D	14.1	Embraer	CFD++/AIPAC
08.1	CIRA	SIMBA	15.1	PolyMtl	CHAMPS
08.2	CIRA	MultiIce	15.2	PolyMtl	CHAMPS
08.3	CIRA	ZEN-IMP3D	16.1	FAA Tech Center	LEWICE / LEWICE3D
08.4	CIRA	Open-Foam	17.1	Honeywell	FENSAP-ICE
09.1	OxfordUniversity	Fluent/ICICLE-2D	19.1	Siemens – Lockheed	Simcenter STAR-CCM+
09.2	OxfordUniversity	Fluent/ICICLE-2D	20.1	Universitat Braunschweig	DICEPS-V3.0/FLUENT
10.1	AIT	CFX/ICEAC2D	20.2	Universitat Braunschweig	DICEPS-V3.0/FLUENT
10.2	AIT	CFX/ICEAC2D	21.1	ATS	Metacomp CFD++
10.3	AIT	CFX/ICEAC2D			

The supplied RANS grids, generated by Dr. Ozcer from Ansys Canada, were used by 10 groups, while 9 created their own meshes and two did not report this metric. Hence, one can infer that RANS technology is often linked to specific mesh generation techniques that correspond to one's solver choice.

For the droplet solver, there were 13 Lagrangian and 13 Eulerian formulations, a fortuitous perfect 50%–50% split showing that none has seen unanimous superiority. The use of SLD models is reported scatteredly, with 5 groups clearly identifying their use.

Ice accretion is achieved via a multi-layer process in 14 of the 21 groups using 2D workflows, and in only 5 of the 13 groups using 3D workflows. Hence, whereas all participants ran 2D cases, only ~60% ran the 3D cases and ~25% ran multi-layer 3D workflows. Two groups used non-deterministic ice accretion models (morphogenetic, stochastic).

Finally, looking at throughput, only 4 groups of the 21 (19%) ran all 8 baseline cases, and 8 groups (38%) ran 6 or more of the 8 cases. The average number of baseline cases ran is 4.6, just above 50% of the 8 baseline cases. It can be concluded that running ice accretion workflows is demanding, even for the very specialized groups that attended the workshop.

A participants information summary is shown in Table 4. The first digit (1–21) is the participant number, and the second is tracking the frameworks used by the participants (1 to as much as 7).

VI. Analysis of Submitted Results

The workshop committee decided to standardize the information contained in specific sets of data such as surface pressure distribution, collection efficiency, ice density and height, geometries, etc. This eased the post-processing activities which remained rather high. Indeed, it is estimated that 1 research associate and 2 Master students at Polytechnique Montreal spent 400 hours producing a 110-page report of comparisons. All workshop presentations, including the 110-page code-to-code comparisons report, are publicly available on the workshop website[†]. The website was created under the leadership of Dr. Hann from Norwegian University of Science and Technology (NTNU). While there are too many data to present in this paper, a subset is shown to provide selected cases that are instructive in drawing conclusions.

[†]www.icepredictionworkshop.com.

A. Cases 111/112: Collection efficiency on swept tail

This first case was selected to provide a validation on a basic configuration, the computation of droplet trajectories only around a swept wing. The experimental and numerical pressure distribution on the clean geometry is presented in Fig. 24, and the collection efficiency is presented in Fig. 25 (case 111) and Fig. 26 (case 112), respectively. The variation in surface pressure distribution is surprising for this non-stalled, subcritical case and is below the standards of other AIAA workshops such as the High-Lift [16] or Drag Prediction [17]. The β–distributions are qualitatively in agreement, but significant discrepancies occur for this simple case. It is no surprise, then, to find even more discrepancies for the similar test case but with larger MVD values, case 112. Quantitatively, the variations between computational results in values of β at $s = -0.1m$ are 0.059 and 0.160 for cases 111 and 112, respectively, which corresponds to a 4–fold increase in the variations. The differences between codes could not be fully explained, as it was not possible to discriminate between all the potential sources of error (different meshes, different types of solvers for aerodynamics and trajectography, possibly different choices of physical conditions such as droplet drag models). For example, there is not even an obvious correlation between the differences observed between the codes on pressure coefficient and β.

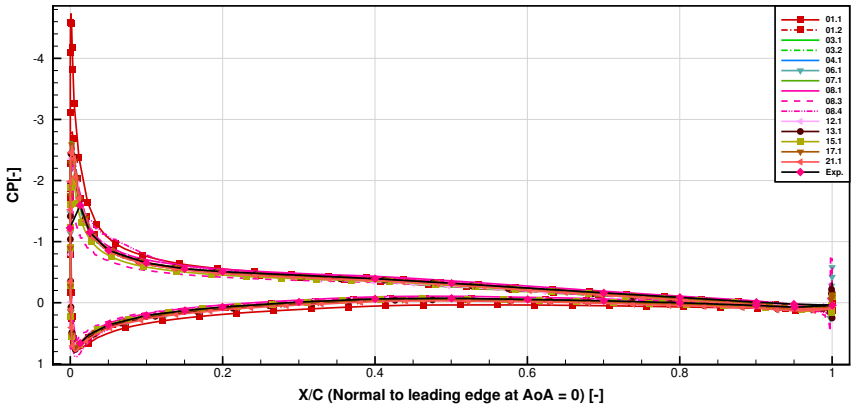

Fig. 24 Case 111 surface pressure distribution.

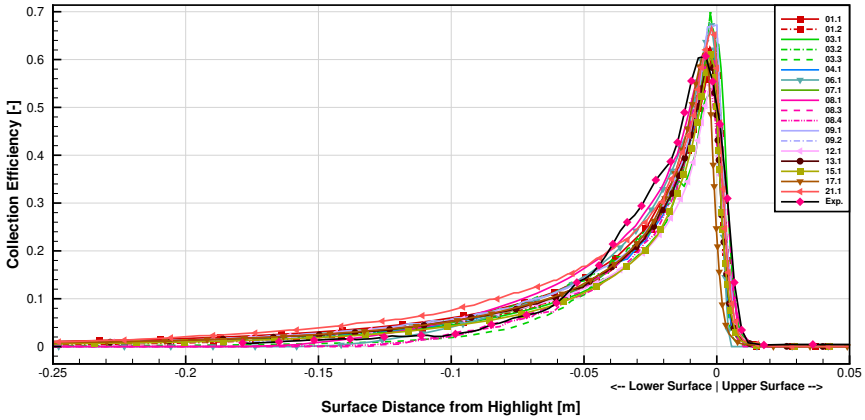

Fig. 25 Case 111 β–distribution.

B. Cases 121/122: Collection efficiency on three–element airfoil

The three–element configuration presents difficulties especially in predicting the aerodynamic flow on the flap. Although some discrepancies were also observed on the slat and on the main element, the errors tend to increase when going further downstream and only the flap analysis is shown here. The 2 cases analyzed here show the influence of droplet size on the collection efficiency for case 121 (Fig. 27) and case 122 (Fig. 28). For the small droplet case,

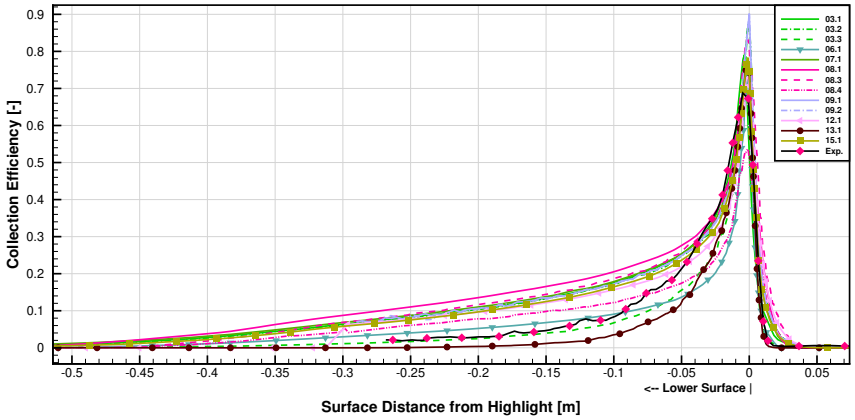

Fig. 26 Case 112 β–distribution.

the workflows agree qualitatively and quantitatively with the experimental values. Indeed, the peak and downstream values at $s = -0.1m$ are overall within 0.1 of the experimental values. However, this gap reaches, at $s = -0.1m$, an underprediction of ~ 0.2 for the large droplet case. A close look at the original data shows that introducing SLD models within the 27–bin distribution reduces this gap, but still with significant differences for $s = -0.05m$.

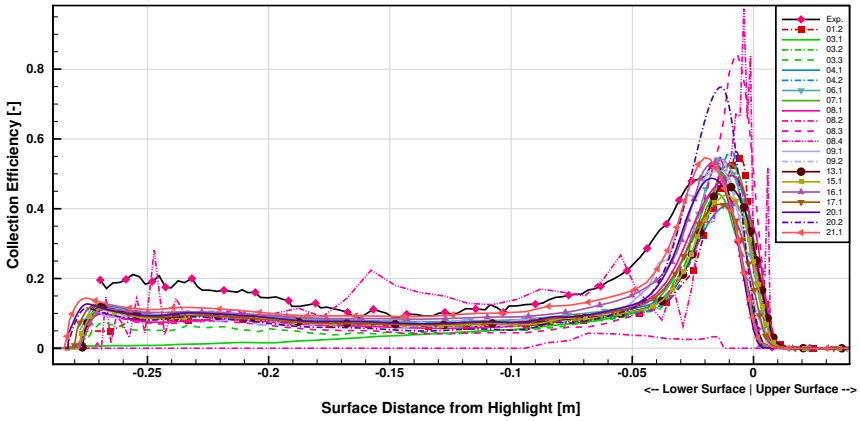

Fig. 27 Case 121 β–distribution.

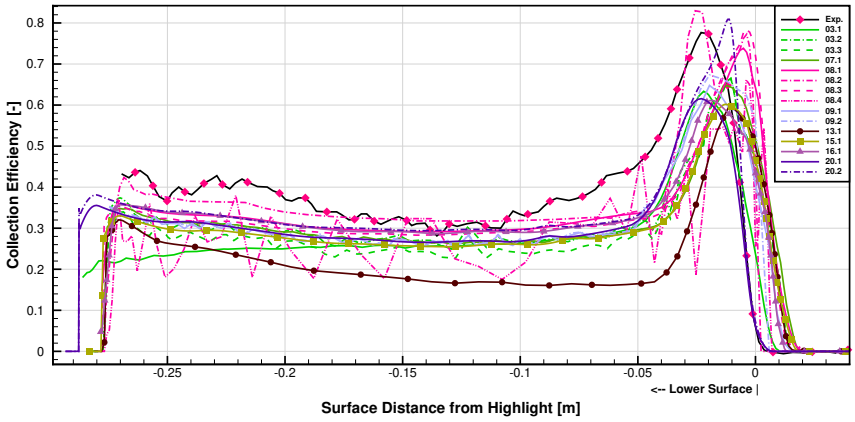

Fig. 28 Case 122 β–distribution.

C. Cases 241/242: Ice accretion on airfoils

These first ice-accretion cases were selected to provide a validation on the simplest case, a 2D airfoil in either rime or glaze conditions. It also constitutes a verification case in between CFD workflows, indicating numerical errors. This case was performed by 18 groups, with 22 solutions owing to the many workflows, and targets ice accretion in rime (case 241) and glaze (case 242) ice conditions. Except for few (3) outliers in Fig. 29, the results for the ice accretion are in good agreement for the rime ice case but vary tremendously for the glaze ice case (also observed in the 2001 RTO/NATO report) . Fig. 31 presents the glaze ice accretion in a segregated fashion to increase clarity. The accreted ice mass, shown in Fig. 30 varies between 0.334 and 0.382 kg/m (12%) and between 0.248 and 0.501 kg/m (50%) for each case, respectively. The convective heat transfer, shown in Fig. 32, shows fourfold differences at $s = 0.02m$ between participants, for both cases (removing one outlier), which partly explains the huge discrepancies in ice shapes since the heat transfer coefficient is known to affect the ice shapes in glaze conditions. It is not a surprise that the glaze-ice case 242 is hardly captured by the codes. The case number 5 investigated by [18–20] in 2017 has very similar characteristics and was already rather poorly reproduced by the codes. Looking closer at the experimental results of case 242, the several runs at NASA show agreement in the region $y \in [-0.0127, 0.0127]$. In particular, the stagnation region with constant ice height ($y \in [0, 0.005]$) is correctly predicted by 18 of the 22 datasets. On the contrary, the shape of the dual horns around $y = -0.0127$ or $y = 0.0127$ is correctly predicted by only 3 of the 22 datasets. It therefore constitutes an excellent case for further studies.

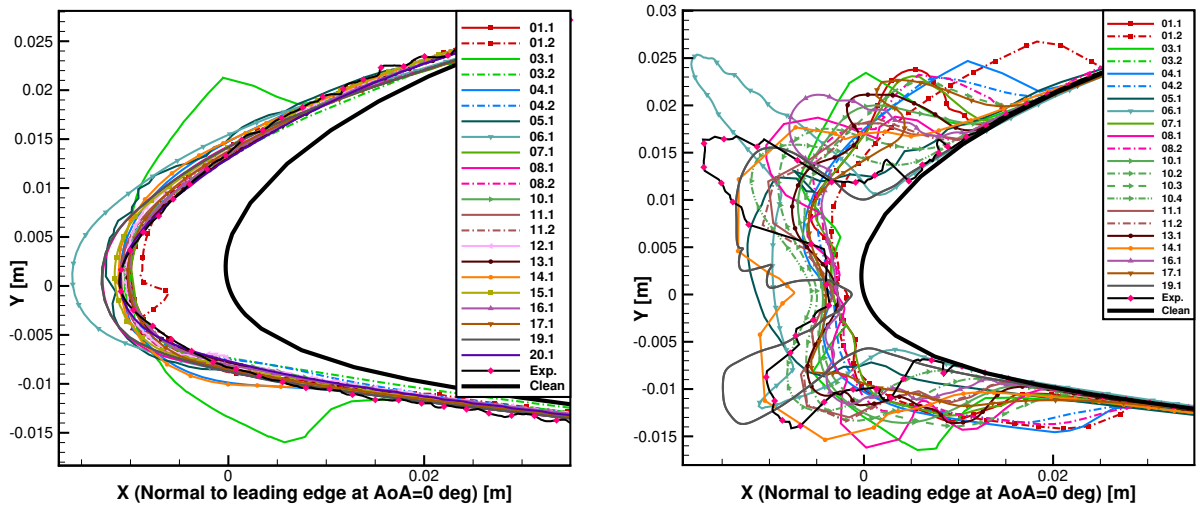

Fig. 29 Ice accretion on airfoil, Case 241 (left), Case 242 (right).

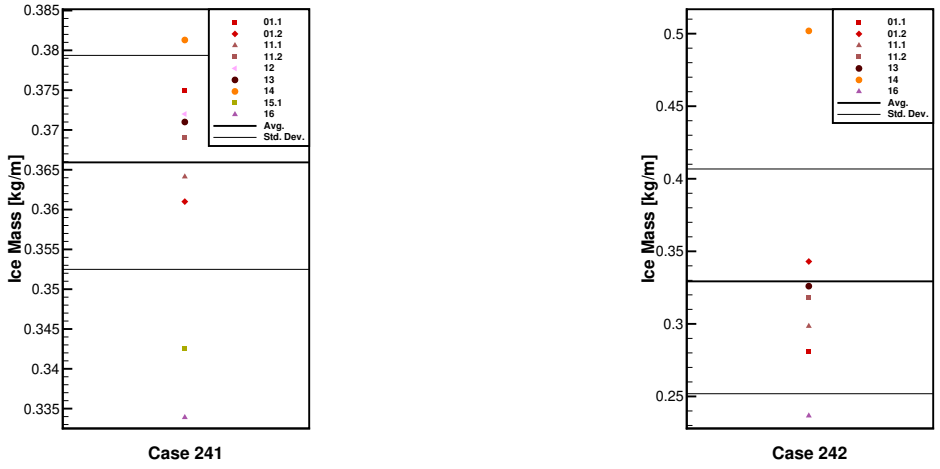

Fig. 30 Ice mass accretion on airfoil, Case 241 (left), Case 242 (right).

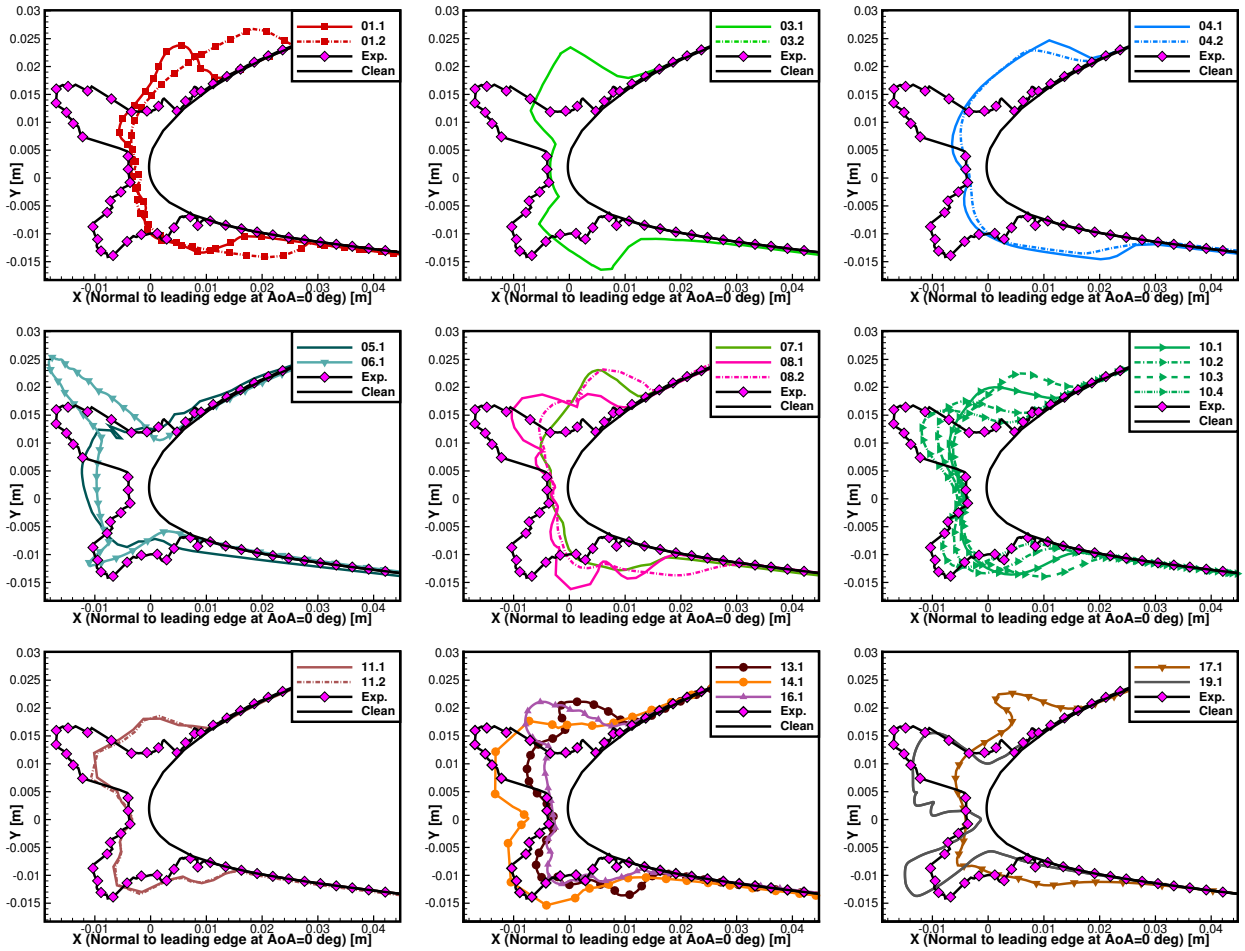

Fig. 31 Ice accretion on airfoil, Case 242 (detailed).

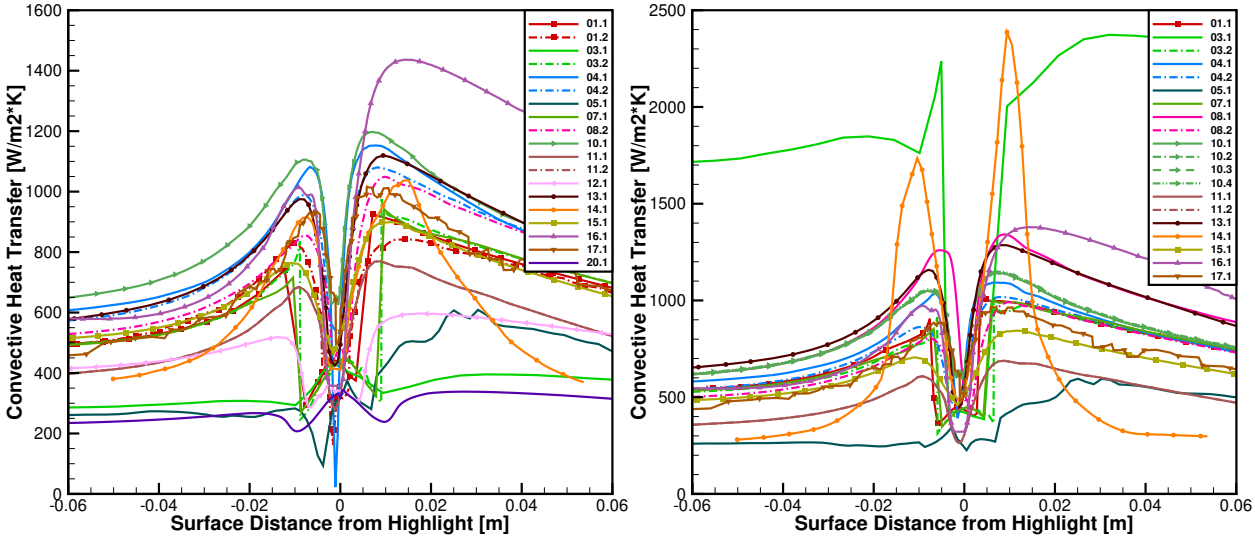

Fig. 32 Convective Heat transfer on airfoil, Case 241 (left), Case 242 (right). Note change of vertical scale.

D. Case 362: Glaze ice accretion on swept wings

The series of cases 361 to 364 examine ice accretion over a 30–degree swept wing in rime and glaze ice conditions. The 4 cases saw, respectively, 16, 13, 6 and 6 data entries. We choose to present case 362, as it possesses many datasets for glaze ice conditions. The other cases can be found in the overall code-to-code comparison report. Looking at the stagnation region at $Y = 0m$ in Fig. 33, 7 entries predict its ice thickness within $\pm 0.01m$ while 6 are outside this range. The vertical ice shape in the region $y \in [-0.05, 0.05]$ is captured by 7 out of the 13 entries. The entries had different models for ice density, shown in Fig. 34: 5 used constant values that varied between 350 and 975kg/m^3, 2 had very small and negligible curvilinear variations and 1 had significant variations between 225 and 850kg/m^3 along the airfoil surface. The collection efficiency, Fig. 34, showed qualitative and quantitative agreement except near the stagnation limits and stagnation point. A close look in the stagnation region, within Fig. 34, shows β values between 0.62 and 0.72. Removing possible outliers, the values oscillate between 0.62 and 0.64. Finally, Fig. 35 shows the convective heat transfer curves. Not only values vary tremendously between 200 and 950 W/(m^2 K), but 2 datasets show stagnation point spikes while 9 show the opposite (i.e. valleys). Removing possible outliers, the differences remain high at 200 W/(m^2 K). The freezing fraction is also shown in Fig. 35, for completeness. One can observe similar tendencies. It can thus be hypothesized that the discrepancies in ice shapes are primarily due to the differences in heat transfer coefficient rather than catch efficiency, and other sources of error which could not be investigated (one-step or multi-step approaches for instance).

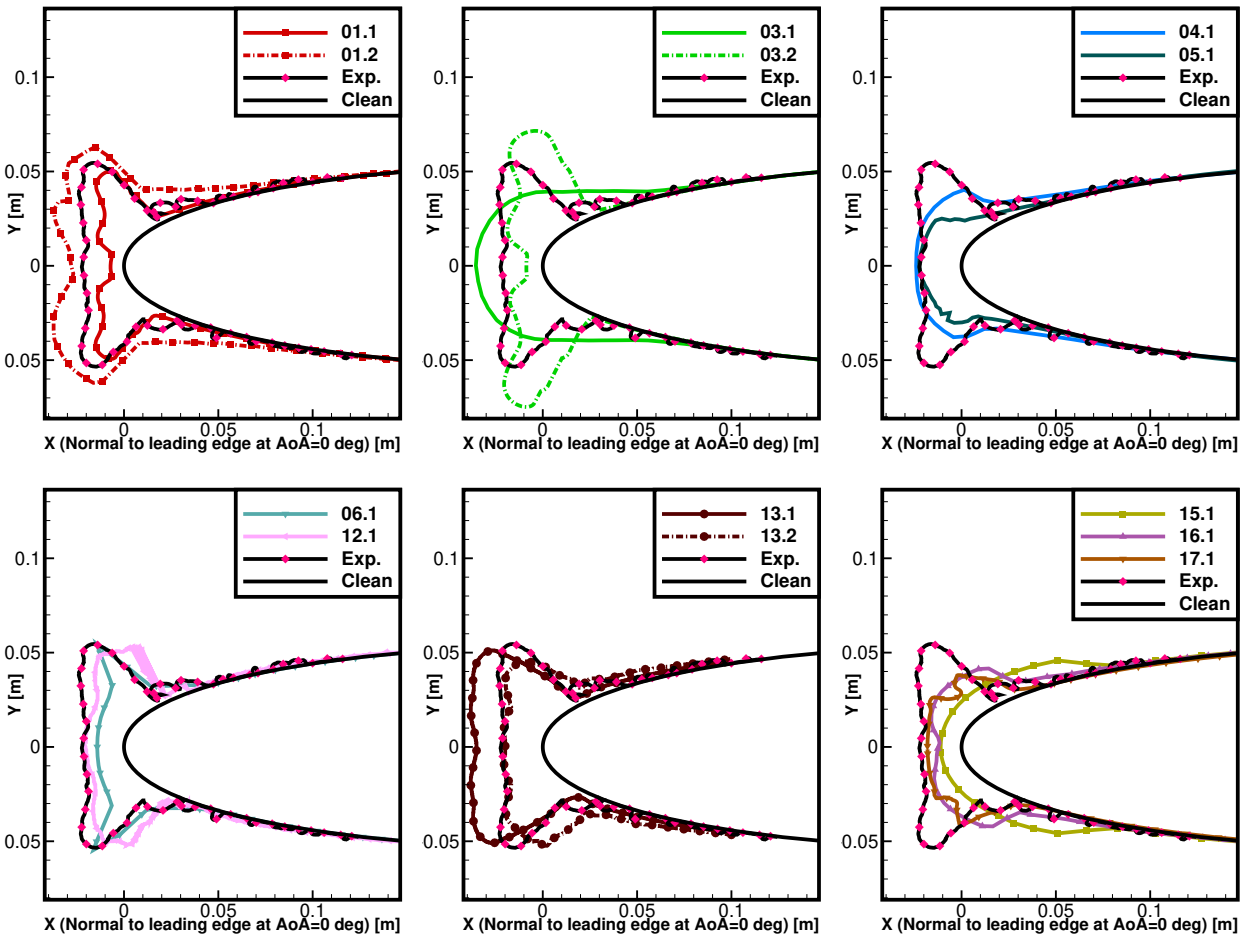

Fig. 33 Ice accretion on swept wing (section), Case 362 (detailed).

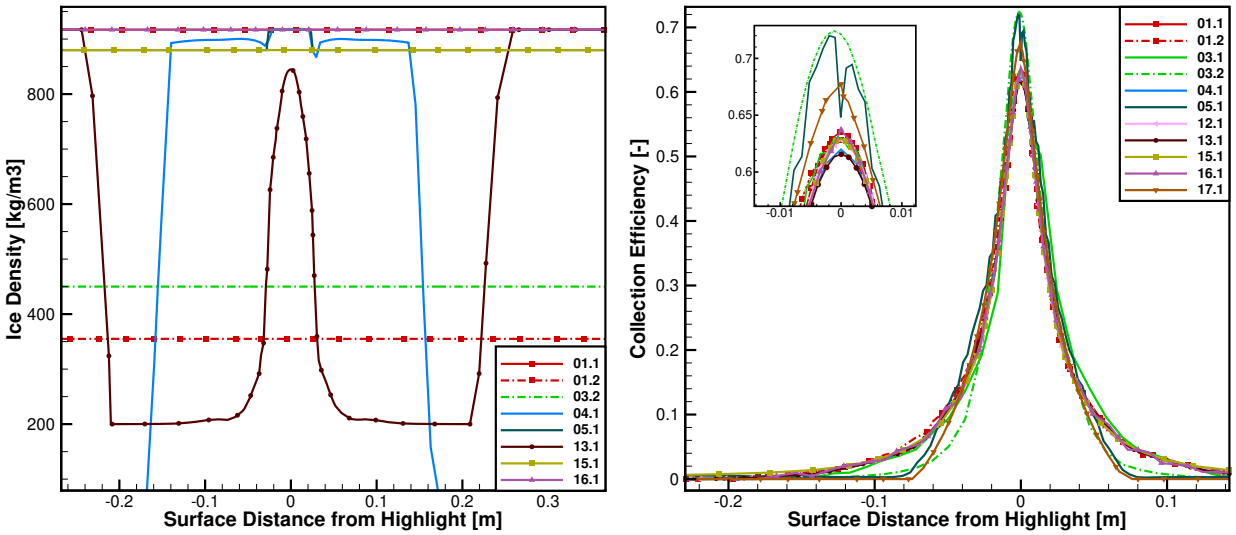

Fig. 34 Case 362, ice density (left) and β–distribution (right) along the swept wing surface (section).

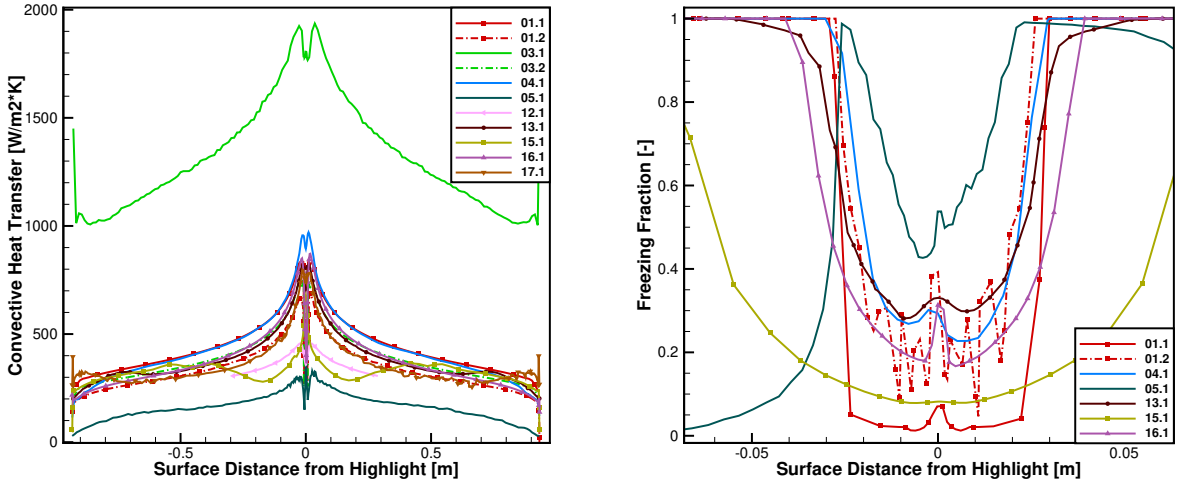

Fig. 35 Case 362, convective heat transfer coefficient (left) and freezing fraction (right) along the swept wing surface (section).

E. Cases 131/132: Collection efficiency on isolated nacelle

The nacelle cases were introduced at the request of scientists working with engines. Only 3 groups, with 4 datasets, provided data. Overall, the comparisons between the numerical and experimental results had similar properties for rime and glaze ice conditions at all nacelle stations (0, 45, 90, 135, 180 degrees). We select case 132, at the 135° station since it is representative of a challenging condition. The nacelle surface pressure distributions, presented as isentropic Mach number on the right of Fig. 36, are well predicted since this is an internal flow problem with specified mass flow rate, hence decoupled from external disturbances. The β–distribution, also in Fig. 36 (left), shows agreement between numerical datasets, and in the stagnation region and positive surface distance from the highlight with the experimental data. However, discrepancies occur in the range $s \in [-0.09, -0.04]$. Other cases show similar trends. Sometimes, the differences between the experiment and the numerical results occurred only in the stagnation region, as shown on Fig. 37 for case 131, for the 0-degree station. One concludes on positive verification of the numerical workflows for this test case, with additional required developments to provide a satisfactory validation.

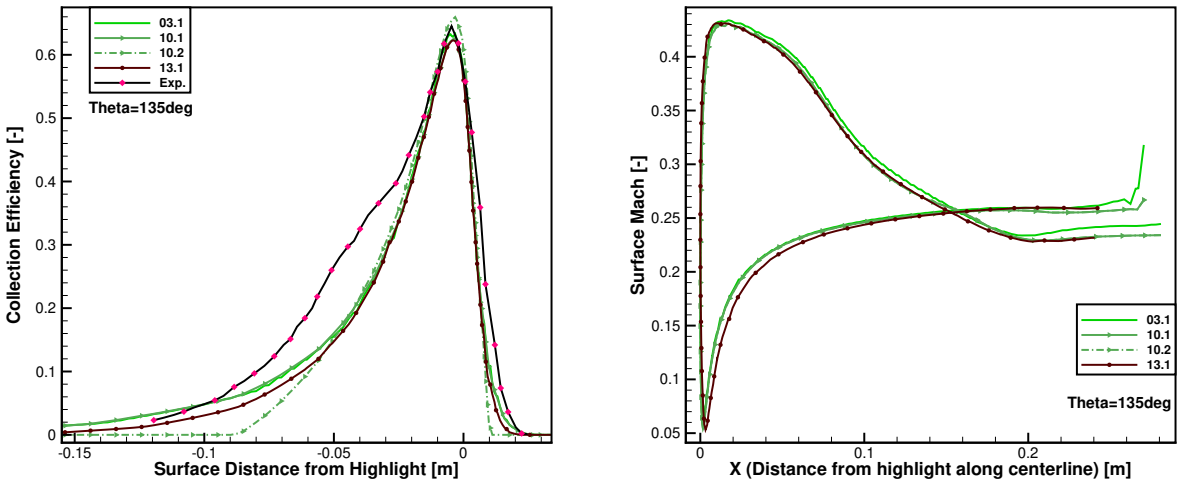

Fig. 36 β–distribution (left) and surface isentropic Mach number (right) along section surface, case 132, theta 135°.

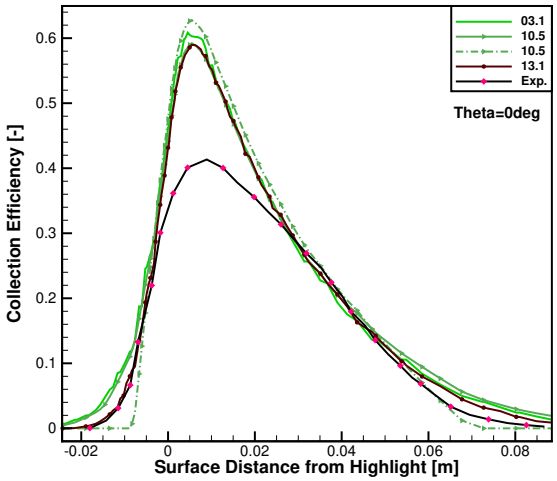

Fig. 37 β–distribution along section surface, case 131, theta 0°.

VII. Conclusion

A diverse committee with members representing several international R&D groups from industry, academia and national centers enacted a four-day workshop to assess the state-of-the-art in ice accretion modelling for applications on aircraft components. The committee offered 8 baseline and 8 optional cases. These encompassed rime ice accretion with water droplet Median Volume Diameters (MVD) of 21 and 92 μm, glaze ice accretion including Supercooled Large Droplets (SLD) with monomodal and bimodal distributions and droplet impingements (so-called β–distributions) for flows over single and multi-element airfoils, wings and nacelles. Standard RANS-grids were provided with participants option to generate their own meshes. Data submitted by 21 participating groups were postprocessed to perform code-to-code (verification) and code-to-experiments (validation) comparisons. The state-of-the-art in terms of methods used has advanced since a similar exercised performed in 2001 during a NATO RTO workshop. Notably, this workshop saw 3D cases while only 2D cases were selected in 2001. Moreover, while 2D and quasi-3D methods (2D with infinite swept wing assumption) are still in use, there are many fully 3D workflows. All 21 presentations but one presented results with the aerodynamic flow modeled via a steady Reynolds-Averaged Navier-Stokes (RANS) solvers. This necessitates the generation of volume grids, which were made available to the participants. Yet, many created their own grids, indicating that grids and solvers sometimes run hand-in-hand. The great majority of participants used a

multi-layer approach, which requires grid deformation techniques. These are readily mature for 2D cases, but not so for 3D cases as only very few participants used multi-layer 3D techniques. The workshop saw novel approaches, such as the immersed boundary method and non-deterministic models. The RANS used either the SA or k-w-SST turbulence models, both well known to be appropriate for external flow aerodynamics. Several workflows used wall roughness to increase the heat transfer rates, and laminar-turbulent transitional models. The droplet solver used a mix of Eulerian and Lagrangian approaches. The use of SLD models remains scarce. The use of multi-bin distributions can be considered standard practice.

Table 5 Standard practices for ice accretion workflows for aircraft applications.

Attribute	2D Workflows	3D Workflows
RANS solver	yes	yes
Potential flow solver	yes	no
Low-Reynolds Turbulence models	yes	yes
Wall roughness	yes	yes
Droplet Solver	mix Lagrangian/Eulerian	mix Lagrangian/Eulerian
Multi-bin distribution	yes	yes
Multi-Layer	yes	no, a few successes
Transition model	no, few successes	No, few successes
Pressure distribution accuracy	yes, but some discrepancies	Not examined
β-distribution	yes, but some discrepancies	yes, but some discrepancies
Heat transfer coefficient	yes, but some discrepancies	yes, but some discrepancies
Freezing fraction	yes, but some discrepancies	yes, but some discrepancies
SLD models	no, few available	no, few available
Running requested Baseline cases	yes	no, still expensive
Ice density model	no, large variations	no, large variations
Experimental error quantification	yes, enough data	no, need more runs
Use of supplied RANS grids	no	no
Common data reporting practices	yes	yes

Based on these observations, some recommendations follow for future workshops:

- A two-year planning scheduled is minimal for organizing the data, producing standard grids, and asking participants to run required cases;
- Reduce the number of baseline cases;
- Strive to understand differences between workflows, i.e., verification. Ask participants to fully describe important workflow metrics, e.g., Far-Field boundary conditions, wall roughness, thermodynamic model terms, SLD models, etc.;
- Assess the effects of experimental uncertainties in the numerical results, including adding recent experimental data or help plan new experimental campaigns;
- Devise one verification case, difficult for this multi-physic problem, examining several key metrics (pressure distribution, collection efficiency, heat transfer coefficient, ice accretion, etc.); Possibly introduce a grid convergence study;
- To reduce postprocessing costs: establish dataset metrics early, reject nonconforming data, refuse data sets after deadline;
- Continue using 2D (error assessment, novel algorithms) and 3D (technology push, industrial pull) validation cases;
- Reduce size of committee, as some members were not actively participating while increasing the effectiveness of the decision-making process;
- Maintain outreach, promote participation from other geographical regions;
- Maintain momentum, as the workshop was found a success based on the feedback from the participants.

Acknowledgments

The authors thank Dr. A. Broeren of NASA for his leadership in making this workshop possible and the AIAA for sponsoring the ice prediction workshop. We thank the dedicated 'Data Analysis Workforce' comprised of Dr. Bourgault-Côté, Mme. Papillon-Laroche, Mr. Blanchet, Dr. Laurendeau, Mr. Cook, Dr. Radenac, Dr. Broeren and Dr. Potapczuk. We acknowledge Polytechnique Montréal Mechanical Engineer department IT team for hosting and setting the secure server. Finally, we thank the committee members and all workshop participants for their contribution towards the workshop objectives.

References

[1] RTO/NATO, "Ice Accretion Simulation Evaluation Test," Tech. rep., North Atlantic Treaty Organization, Nov. 2001.

[2] Papadakis, M., Hung, K. E., Vu, G. T., Yeong, H. W., Bidwell, C. S., Breer, M. D., and Bencic, T. J., "Experimental Investigation of Water DropletImpingement on Airfoils, Finite Wings,and an S-Duct Engine Inlet," Tech. rep., NASA TM 2002-211700, Oct. 2002.

[3] Papadakis, M., Elangonan, R., Freund, J., G. A., Breer, M., Zumwalt, G. W., and Whitmer, L., "An Experimental Method for Measuring Water Droplet Impingement Efficiency on Two- and Three-Dimensional Bodies," Tech. rep., NASA CR 4257, Nov. 1989.

[4] Lee, S., Broeren, A. P., Kreeger, R. E., Potapczuk, M. G., and Utt, L., "Implementation and Validation of 3-D Ice Accretion Measurement Methodology," *6^{th} AIAA Atmospheric and Space Environments Conference*, AIAA Paper 2014-2613, 2014. https://doi.org/10.2514/6.2014-2613.

[5] Potapczuk, M., and Tsao, J., "The Influence of SLD Drop Size Distributions on Ice Accretion in the NASA Research Tunnel," *SAE 2019 International Conference on Icing of Aircraft, Engines, and Structures*, SAE Technical Paper 2019-01-2022, 2019. https://doi.org/10.4271/2019-01-2022.

[6] Bidwell, C. S., "Icing Analysis of a Swept NACA 0012 Wing Using LEWICE3D Version 3.48," *6^{th} AIAA Atmospheric and Space Environments Conference*, AIAA Paper 2014-2200, 2014. https://doi.org/10.2514/6.2014-2200.

[7] Potapczuk, M. G., and Tsao, J.-C., "Bimodal SLD Ice Accretion on Swept NACA 0012 Airfoil Models," *AIAA Aviation 2020 FOrum*, AIAA Paper 2020-2814, 2020. https://doi.org/10.2514/6.2020-2814.

[8] Szilder, K., and Lozowski, E. P., "NSimulation of Airfoil Icing with a Novel Morphogenetic Model," *Journal of Aerospace Engineering*, Vol. 18, No. 2, 2005, pp. 102–110. https://doi.org/10.1061/(ASCE)0893-1321(2005)18:2(102).

[9] Papillon Laroche, H., Bourgault-Côté, S., and Laurendeau, E., "Multi-Layer Stochastic Ice Accretion Model for Aircraft Icing," *AIAA Aviation 2021 FOrum*, AIAA Paper 2021-2629, 2021. https://doi.org/10.2514/6.2021-2629.

[10] Broeren, A. P., Potapczuk, M. G., Lee, S., Malone, A. M., Paul, B. P., and Woodard, B., "Ice-Accretion Test Results for Three Large-Scale Swept-Wing Models in the NASA Icing Research Tunnel," *8^{th} AIAA Atmospheric and Space Environments Conference*, AIAA Paper 2016-3733, 2016. https://doi.org/10.2514/6.2016-3733.

[11] Pena, D., Hoarau, Y., and Laurendeau, E., "A single step ice accretion model using Level-Set method," *Journal of Fluids and Structures*, Vol. 65, 2016, pp. 278–294. https://doi.org/10.1016/j.jfluidstructs.2016.06.001.

[12] Spalart, P. R., and Allmaras, S. R., "A One-Equation Turbulence Model for Aerodynamic Flows," *Recherche Aerospatiale*, Vol. 94, No. 1, 1994, pp. 5–21.

[13] Menter, F. R., "Two-Equation Eddy-Viscosity Turbulence Models for Engineering Applications," *AIAA Journal*, Vol. 32, No. 8, 1994, pp. 1598–1605. https://doi.org/10.2514/3.12149.

[14] Braslow, A. L., Harris, J., R. V., and Hicks, R. M., "Use of grit-type boundary-layer transition trips on wind-tunnel models," Tech. rep., NASA–TN–D–3579, Sep. 1966.

[15] Menter, F. R., Langtry, R. B., Likki, S. R., Suzen, Y. B., Huang, P. G., and Völker, S., "A Correlation-Based Transition Model Using Local Variables—Part I: Model Formulation," *Journal of Turbomachinery*, Vol. 128, No. 3, 2004, pp. 413–422. https://doi.org/10.1115/1.2184352.

[16] Rumsey, C. L., Slotnick, J. P., and Sclafani, A. J., "Overview and Summary of the Third AIAA High Lift Prediction Workshop," *Journal of Aircraft*, Vol. 56, No. 2, 2019, pp. 621–644. https://doi.org/10.2514/1.C034940.

[17] Tinoco, E. N., Brodersen, O. P., Keye, S., et al., "Summary Data from the Sixth AIAA CFD Drag Prediction Workshop: CRM Cases," *Journal of Aircraft*, Vol. 55, No. 4, 2018, pp. 1352–1379. https://doi.org/10.2514/1.C034409.

[18] Trontin, P., Blanchard, G., Kontogiannis, A., and Villedieu, P., "Description and assessment of the new ONERA 2D icing suite IGLOO2D," 9^{th} *AIAA Atmospheric and Space Environments Conference*, AIAA Paper 2017-3417, 2017. https://doi.org/10.2514/6.2017-3417.

[19] Wright, W. B., and Porter, C. E., "A Revised Validation Process for Ice Accretion Codes," 9^{th} *AIAA Atmospheric and Space Environments Conference*, AIAA Paper 2017-3415, 2017. https://doi.org/10.2514/6.2017-3415.

[20] Han, Y., Rocco, E., and Palacios, J., "Validation of a LEWICE-based Icing Code with Coupled Heat Transfer Prediction and Aerodynamics Performance Determination," 9^{th} *AIAA Atmospheric and Space Environments Conference*, AIAA Paper 2017-3416, 2017. https://doi.org/10.2514/6.2017-3416.